

Defects dynamics following thermal quenches in square spin-ice

Demian Levis^{1,2} and Leticia F. Cugliandolo¹

¹*Université Pierre et Marie Curie - Paris 6, Laboratoire de Physique Théorique et Hautes Energies, 4, Place Jussieu, Tour 13, 5ème étage, 75252 Paris Cedex 05, France*

²*Laboratoire Charles Coulomb, UMR 5221 CNRS and Université Montpellier 2, Montpellier, France*

We present a study of the single spin flip stochastic dynamics of the two dimensional sixteen vertex model. We single out several dynamic regimes controlled by different processes that we describe. We analyse the emergence of very long-lived metastable states and their dependence on the system size, boundary conditions, and working parameters. We investigate the coarsening process after quenches into the ordered ferromagnetic and antiferromagnetic phases. We discuss our results in the context of artificial spin ice on square lattices.

PACS numbers: 75.10.Hk, 05.70.Ln, 75.40.Lk, 75.40.Mg

CONTENTS

I. Introduction	1
II. Model and methods	2
A. The sixteen-vertex model	2
B. Stochastic dynamics	3
C. Quench dynamics	3
D. Observables	4
III. Defect density	4
A. Quench into the PM phase	4
1. Equally probable defects, $d = e$.	4
2. Single charged defects are more favourable than doubly charged ones, $d < e$.	5
3. Boundary conditions	5
4. Finite size effects	6
5. Initial decay	6
B. Quench into the FM phase	6
C. Quench into the c -AF phase	7
D. Conclusion	7
IV. Coarsening dynamics and ageing	8
A. Slow relaxation towards the PM phase	8
B. Anisotropic FM domain growth	8
C. Isotropic c -AF domain growth	10
1. c -AF sixteen-vertex model with $d = e^2$	10
2. Artificial Spin Ice	12
V. Conclusion	12
References	13

I. INTRODUCTION

Frustrated magnets are classical and quantum systems in which the interactions in combination with the lattice structure impede the spins to order in an optimal configuration at zero temperature [1]. In classical instances, the local minimisation of the interaction energy on a frustrated unit gives rise to a macroscopic degeneracy of the ground state. This occurs in spin-ice samples in which the spin interactions mimic the

frustration of proton positions in water ice. The theoretical interest in these systems has been boosted in recent years by the artificial design of materials. For instance, regular arrays of elongated single-domain ferromagnetic nano-islands arranged along the sides of a $2D$ square lattice, were manufactured. The beauty of artificial spin-ice (ASI) is that the state of a single degree of freedom can be directly visualised with magnetic force microscopy. Moreover, advances in lithography allow great flexibility in their design, and the interaction parameters can be precisely controlled by tuning the island length, the distance between them, and the height between layers, to select the phase into which the system should set in [2–4]. One of the main goals of the research on artificial spin-ices is to develop new materials that could improve the performance of data storage and data processing devices [5, 6].

One can model spin-ice materials by taking into account dipolar interactions [7–10] or by using a simpler vertex model [3, 11, 12]. In perfect spin-ice samples the total spin surrounding a lattice point is constrained to vanish according to the two-in/two-out rule, and the vertex model is integrable. For the model defined on a square lattice two ordered and a critical disordered (spin liquid) phase have been found with powerful analytic tools [13, 14]. The model with four-in or four-out arrows can also be solved analytically and the critical character of the disordered phase is lost in this case [15]. Vertices that do not satisfy the two-in/two-out rule and carry dipolar moment break integrability and no exact tool exists to solve models with them. We recently solved the statics of the sixteen-vertex (all possible states of four arrows attached to a central site) model with an extension of the Bethe-Peierls or cavity method [12] and we found intriguing relations between this technique and the ones of integrable systems.

In this work, we will be interested in characterising the *single spin flip stochastic dynamics* of the sixteen vertex model on a two dimensional square lattice with energetically unfavored defects. Indeed, classical natural frustrated magnets are subject to thermal fluctuations, and these can be captured by vertex models coupled to a heat-bath [11, 16]. In a previous Letter we showed that their stochastic dynamics display metastability in the disordered phase, coarsening of stripes in the ferromagnetic phase, and growth of domains, that can be made isotropic, in the antiferromagnetic phase [11]. Here, we extend this analysis in several directions to be described in de-

tail in the main text. We work with system sizes $L = O(10^2)$ that are of the same order as the ones manufactured with lithography techniques when preparing artificial spin-ice samples. Finite size effects observed in the simulations are then relevant to observations in these materials.

The manuscript is organised as follows: we first present the model and the simulation method in Section II; next, in Section III, we discuss the possibility to set the system in metastable states with constant number of vertices of each kind and an excess of defects following different quenches into the PM (Section III A), a -FM (Section III B) and c -AF (Section III C) phases. In Section IV we report our results on the coarsening dynamics occurring in the model following the before mentioned procedure into the a -FM phase (Section IV B) and c -AF phase (Section IV C). Finally, in Sect. V we present our conclusions.

II. MODEL AND METHODS

In this Section we present the model and the numerical techniques used in this work.

A. The sixteen-vertex model

Conventional vertex models are defined on a finite dimensional lattice, typically a square one. The degrees of freedom (Ising spins, q -valued Potts variables, etc.) sit on the edges of the lattice. In our case we use an $L \times L$ bidimensional square lattice \mathcal{V} with unit spacing and periodic boundary conditions (PBC). The midpoints of the edges of the lattice \mathcal{V} constitute another square lattice, the medial lattice $\hat{\mathcal{V}}$. In the following we label the sites of $\hat{\mathcal{V}}$ with (i, j) , see Fig. 1. In the model we focus on, the degrees of freedom are arrows aligned along the edges of the original square lattice \mathcal{V} . We can think of them as Ising spins $s_{ij} = \pm 1$. Without loss of generality, we choose a convention such that $s = +1$ corresponds to an arrow pointing in the right or up direction, depending on the orientation of the link; conversely, $s = -1$ corresponds to arrows pointing down or left. When the spins joining at each vertex of \mathcal{V} are constrained to satisfy the two-in/two-out rule [17, 18], as for the first six vertices in Fig. 2, one has the *six-vertex* model. When the next two vertices in this figure are also allowed (four-in and four-out arrows) one has the *eight-vertex* model. Otherwise, the model is generalized to allow for all possible vertices with four legs and becomes the *sixteen-vertex* one, that we have already studied in [11, 12, 19]. A *charge*, q , defined as the number of out-going minus the number of incoming arrows, can be attributed to each single vertex configuration [20, 21]. Accordingly, in the six-vertex model vertices have zero charge and all other vertices breaking the ice-rule have a net (positive or negative) charge.

The energy of each vertex configuration is quantified by the Hamiltonian $H = \sum_{k=1}^{16} \epsilon_k n_k$, where n_k is the number of vertices of type k and ϵ_k its energy. We assign a (not normalized) Boltzmann weight $\omega_k = e^{-\beta \epsilon_k}$ to each of the $k = 1, \dots, 2^4$ four-arrow vertex configurations (note that ω_k

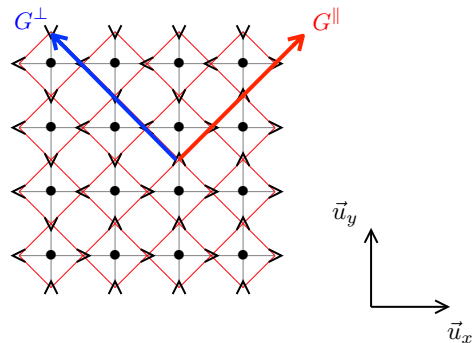


Figure 1. (Colour online.) The original lattice \mathcal{V} , with L^2 vertices, is shown in grey. Its medial lattice, $\hat{\mathcal{V}}$, with $2L^2$ spins is shown in red. The Cartesian system of coordinates of the original lattice (\vec{u}_x, \vec{u}_y) is shown in the right bottom end and the $(\pi/4)$ -rotated Cartesian system of coordinates used to compute parallel and perpendicular correlation functions is displayed on the lattice.

can be greater than one if ϵ_k is negative). We set $\omega_1 = \omega_2 = a$, $\omega_3 = \omega_4 = b$, $\omega_5 = \omega_6 = c$ for the ice-rule vertices and $\omega_7 = \omega_8 = d$, $\omega_9 = \dots = \omega_{16} = e$ for the 2-fold and 1-fold defects, respectively, ensuring invariance under reversal of all arrows (see Fig. 2).

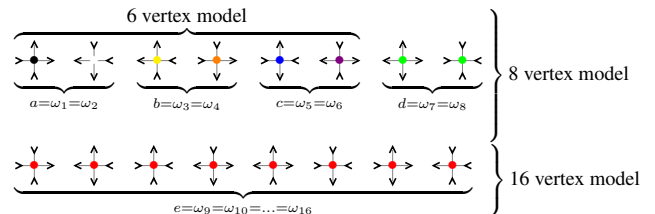


Figure 2. (Colour online.) The sixteen vertex configurations on the $2D$ square lattice and their weights. The first six vertices verify the ice-rule. The next pair (2-fold defects) completes the eight-vertex model and have charge $q = \pm 2$. The last eight vertices (1-fold defects) have charge $q = \pm 1$.

The static phase diagram of this model was obtained in [12] by using the cavity analytic method (Bethe-Peierls approximation) and numerical simulations on $2D$. We will not repeat all the results found in this (long) paper but we simply recall that for $d \neq 0$ and $e \neq 0$ the model has a complex phase diagram with many phases. In particular, we singled out a conventional disordered paramagnetic (PM) phase, two ferromagnetic (FM) phases (a and b dominated, respectively), and two antiferromagnetic (AF) phases (c and d dominated, respectively). All transitions are of second order if $d \neq 0$ and $e \neq 0$. Using numerical simulations, FM order dominated by a vertices was found for $a \gtrsim b + c + d + 3e$, close to the critical line predicted by the analytic calculations. Using the same arguments, AF order dominated by c vertices was found for $c \gtrsim a + b + d + 3e$ and the PM phase was found for $a, c, d, e \lesssim \frac{1}{2}(a + b + c + d + 3e)$ (for the precise prediction, that we give here only in approximate form, see [11]). For small defect weight, $e, d \ll a, b, c$ the disordered phase is very close to the *critical* spin-liquid phase of the six-vertex model. The closeness to criticality will play an important role in quenches

into the disordered phase. Henceforth we measure the weights in units of c : $c \rightarrow 1$ and $a, b, d, e \rightarrow a/c, b/c, d/c, e/c$.

B. Stochastic dynamics

We mimic the effect of thermal fluctuations in spin-ice samples by coupling the model to an environment and allowing for *local single spin flips* determined by the heat-bath rule. Local moves that break the spin-ice rule are not forbidden and we therefore allow for thermally-activated creation of defects. The dynamics do not conserve any of the various order parameters, and are ergodic for both fixed and periodic boundary conditions. We establish a Monte Carlo algorithm and we define the unit of time as a Monte Carlo sweep (MCs). In systems with frustration, as the one we are dealing with, computer time is wasted by the large rejection of blindly proposed updates. In order to make the computer time dynamics faster we use a rejection-free continuous-time Monte Carlo (MC) algorithm [22]. The longest time that we reached with this method, once translated in terms of usual MC sweeps, is of the order of 10^{25} MCs, a scale that is unreachable with usual Metropolis algorithms.

Other kinds of dynamic rules have been used in the literature, with different purposes. For instance, a rule that preserves the ice constraint does not create defects. In order to sample the whole phase space on a system with PBC in this way one needs to introduce loop updates of any size and winding number. Such a dynamics have been studied in the 3-colouring model on the hexagonal lattice and leads to glassy behavior [23, 24]. Another possible local dynamics which preserve the ice rules would be to update the system by small loops made by four spins around a square plaquette. These dynamics are not ergodic for PBC but they are for the six-vertex model with domain-wall BC (DWBC) [25, 26]. For the spin-ice problem, these two possible dynamical models seem quite artificial and do not allow us to study defects' motion in the way that it is observed to occur in the laboratory. We therefore attach to the moves described in the previous paragraph.

In terms of a reaction-diffusion model the relevant processes taking place during the time-evolution are:

$$(2q) + (-2q) \rightarrow (q) + (-q), \quad \Delta E \propto 2k_B T \ln(d/e), \quad (1)$$

$$(2q) + (-q) \rightarrow (q) + (0), \quad \Delta E \propto k_B T \ln(d/a), \quad (2)$$

$$(q) + (q) \rightarrow (2q) + (0), \quad \Delta E \propto k_B T \ln(e^2/bd), \quad (3)$$

$$(q) + (-q) \rightarrow (0) + (0), \quad \Delta E \propto k_B T \ln(e^2/ab), \quad (4)$$

where the energetic change ΔE associated with each reaction is shown. As $\Delta E = E_F - E_I$, with $E_F = k_B T \ln \omega_F^{-1}$ the energy of the final configuration and $E_I = k_B T \ln \omega_I^{-1}$ the energy of the initial configuration, one has $\Delta E = k_B T \ln(\omega_I/\omega_F)$. In our simulations we will typically use $a, b \gg e \geq d$ as this choice is more relevant experimentally. In the first case, eq. (1), two defects of type 7 and 8 meet to produce two singly (and oppositely) charged defects with an energetic gain, if $e > d$, which depends on the ratio e/d . The total density of defects remains constant after this reaction although their type changes. An example of the second

case, eq. (2), is shown in Fig. 3: a defect of type 7 (charge $q = 2$) meets one of type 14 (charge $q = -1$) to produce a defect of type 10 (charge $q = 1$) and a spin-ice vertex of type 2 with no charge. This corresponds to an energetic gain $\Delta E < 0$ which depends on d/a . Note that the number of single charged defects has not been modified during this process but the number of doubly charged defects diminished and so did the total number of defects. The reaction in the third line represents an initial state made of the 13th vertex (on the left) and the 15th vertex (on the right) that turn into a state with the 3rd vertex (on the left) and the 7th vertex (on the right) by reversing the internal link. The energy variation is then $\Delta E = k_B T \ln(e^2/bd)$, and this can be positive or negative depending on e/b (smaller than one) vs. e/d (larger than one). The fourth reaction is realised, for example, by the reversal of the spin on the edge linking vertex number 13 (on the left) with vertex number 14 (on the right), leading to vertex number 3 (on the left) and vertex number 2 (on the right). The energy change is then $\Delta E = k_B T \ln(e^2/ab)$, a negative quantity for our choice of parameters.

In conclusion, with our choice of parameters, the reactions in eqs. (1), (2) and (4) lead to a decrease in energy while the reaction in eq. (3) may be energetically favourable or not depending on the ratio e^2/bd .

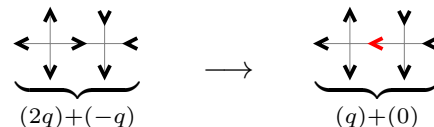


Figure 3. (Colour online.) The reaction in eq. (2).

C. Quench dynamics

We will analyse the system's evolution after an infinitely rapid quench from a disordered initial condition into the disordered (D), a -ferromagnetic (a -FM) and c -antiferromagnetic (c -AF) phases. In practice, we choose a completely disordered configuration ($T_0 \rightarrow \infty$, $a = b = d = e = 1$) as an initial condition; such a state is constructed by placing arrows at random on each edge of the square lattice \mathcal{V} . If we impose PBC, the number of positive and negative charges is identical. We subsequently evolve the MC code with parameters that belong to the three interesting phases. The system remains globally neutral during the evolution, since it is updated by single spin flips which cannot create any excess of charge.

After a quench into the disordered phase the system could be expected to equilibrate relatively rapidly; still, it was shown in [11] that it remains blocked in metastable states with a finite density of defects for long times, if the weight of defects is low enough. We will investigate this problem in depth here. We will demonstrate that metastability also exists after quenches into the ordered phases. Eventually, the interactions between the spins, mediated by the choice of vertex weights, creates ordered domains of FM or AF kind. The quantitative characterisation of growth in the ordering processes is given by two

possibly different growing lengths extracted from correlation functions along orthogonal directions \parallel and \perp that we identify in Fig. 1.

D. Observables

The relaxation dynamics of clean lattice systems are usually studied in terms of time-dependent macroscopic observables averaged over different realisations of the dynamics (thermal noise, initial conditions) denoted by $\langle \dots \rangle$. In particular, we compute the following quantities:

(i) The *density of vertices* of each type:

$$n_a(t) = \langle n_1(t) + n_2(t) \rangle, n_b(t) = \langle n_3(t) + n_4(t) \rangle, \quad (5)$$

$$n_c(t) = \langle n_5(t) + n_6(t) \rangle, \quad (6)$$

$$n_d(t) = \langle n_7(t) + n_8(t) \rangle, n_e(t) = \left\langle \sum_{k=9}^{16} n_k(t) \right\rangle, \quad (7)$$

$$n_{def}(t) = n_d(t) + n_e(t). \quad (8)$$

(ii) The *two-times self-correlation function* defined by:

$$C(t, t_w) = \frac{1}{2L^2} \sum_{(i,j) \in \hat{\mathcal{V}}} \langle S_{(i,j)}(t) S_{(i,j)}(t_w) \rangle \quad (9)$$

with $t > t_w$. The indices (i, j) denote the coordinates of an Ising spin in the medial lattice $\hat{\mathcal{V}}$ (i.e. the vertices of the square lattice shown in red in Fig. 1).

(iii) The *space-time correlation functions*. The definition of the relevant correlation functions between different points in the lattice is not straightforward when we introduce some anisotropy in the model (for example, by choosing $a > b$). For convenience, we define a set of correlation functions between spins using two different orientations: along the Cartesian axes \vec{u}_x and \vec{u}_y and along the $\pi/4$ -rotated axes \vec{u}_{\parallel} and \vec{u}_{\perp} (see Fig. 1). The space-time self correlation functions along \vec{u}_{\parallel} and \vec{u}_{\perp} are defined as

$$G^{\parallel}(r = n, t) = \frac{1}{L^2} \sum_{(i,j) \in \hat{\mathcal{V}}} \langle S_{(i,j)} S_{(i,j+n)} \rangle, \quad (10)$$

$$G^{\perp}(r = n, t) = \frac{1}{L^2} \sum_{(i,j) \in \hat{\mathcal{V}}} \langle S_{(i,j)} S_{(i+n,j)} \rangle, \quad (11)$$

where $n \in \mathbb{N}$.

(iv) The *growing lengths* $L^{\parallel}(t)$ and $L^{\perp}(t)$ along \vec{u}_{\parallel} and \vec{u}_{\perp} are extracted numerically from the scaling of the space-time correlations:

$$G^{\parallel,\perp}(r, t) \simeq F_{G^{\parallel,\perp}} \left(\frac{r}{L_{\parallel,\perp}(t)} \right). \quad (12)$$

III. DEFECT DENSITY

In this Section we study the density of defects, vertices of type e and d after quenches into the different phases. With this analysis we investigate the possibility of finding long-lived metastable states after dynamic quenches from a fully disordered initial condition.

A. Quench into the PM phase

In the following, we study the evolution of the model after a quench from a random initial condition ($a = b = d = e = 1$) into a different PM state, typically close to the SL critical phase (i.e. $a = b = 1$ and $d, e \ll 1$). In the initial configurations defects are common: we are interested here in the mechanisms leading to their annihilation.

1. Equally probable defects, $d = e$.

The evolution of the system after a sudden quench into the PM phase with $d = e$ was already reported in [11]. Let us recall some useful results: for values of d large enough ($d = e \geq 10^{-4}$) the density of defects n_{def} quickly saturates to its equilibrium value. For smaller d 's, the system gets arrested into a metastable state with finite and constant density of defects $n_{def} = n^p$ for long periods of time. This dynamical plateau lasts longer for smaller d s, a behaviour reminiscent to what was found in 3D dipolar spin-ice [27]. The time regime where the density of defects finally leaves the plateau and reaches its equilibrium value, is characterised by a scaling of the dynamic curves with the characteristic time d^{-2} . This scaling strongly suggests that the relevant time scale in the system is the typical time needed to create a pair of single defects. From an ice-rule state, the energy change associated with the reaction: $(0) + (0) \rightarrow (q) + (-q)$ is, e.g., $\Delta E \propto -k_B T \ln(d^2/ab)$, with $a = b = 1$ in the simulation. Then, by a simple Arrhenius argument, the typical time needed in order to overcome this barrier is $\propto \exp(\beta \Delta E)$ giving the before mentioned time-scale $\tau \propto d^{-2}$.

At a first sight, one could think that the emergence of this dynamical plateau in the density of defects is due to the presence of doubly charged defects, the ones with $q = \pm 2$ and weights $\omega_7 = \omega_8 = d$. Indeed, doubly charged defects 7 and 8 must decay into two single charged defects in order to be able to move. However, the inverse reaction $(2q) + (0) \rightarrow (q) + (q)$ in eq. (3) is accompanied by an increase in energy, $\Delta E \propto k_B T \ln(b/d) > 0$ when $d = e$, and it is energetically unfavourable. Therefore, d -vertices get naturally stuck in the sample and are very hard to eliminate. This mechanism could give a justification for the plateau in the case $d = e$.

In real spin-ice realisations, both in 2D and 3D, the energy associated to doubly charged defects is much larger than the one of single charged ones $\epsilon_{7,8} \gg \epsilon_{9,\dots,16}$. It is then more relevant to experiments to study in detail the effect of $d < e$ in the time evolution of the model, and to revisit the influence of e and d defects on the development of the plateau.

2. *Single charged defects are more favourable than doubly charged ones, $d < e$.*

We investigate now the dynamical consequences of choosing different weights for the two kinds of defects. We focus on the fate of the dynamical plateau when doubly charged defects are rapidly suppressed, with d the smaller weight in the model. The inspection of the reaction rates for the annihilation-creation of defects suggests to study the two following cases separately:

- $d < e$ and $d > e^2$: Single charged defects e are slightly more favourable than d -defects. However, the decay of d -defects into two e -defects following the inverse reaction eq. (3) must overcome an energy barrier, as $\Delta E = k_B T \ln(bd/e^2) > 0$.
- $d < e$ and $d < e^2$: Doubly charged defects are very unfavourable. The decay of d -defects into two e -defects is energetically favoured and occurs spontaneously.

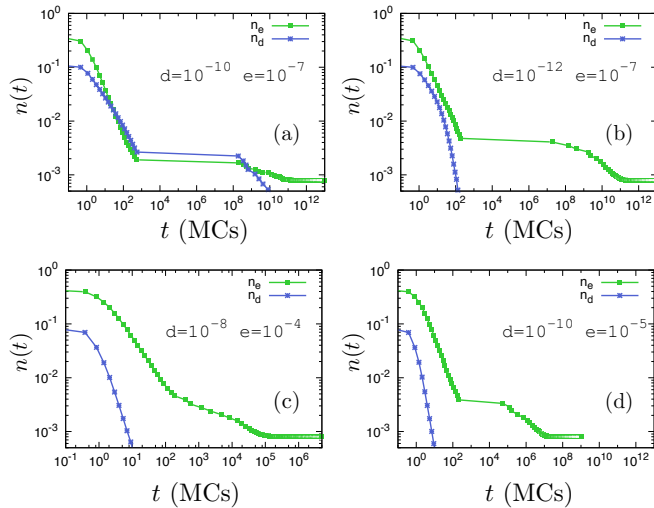


Figure 4. (Colour online.) Quench into the PM phase. Decay of the density of vertices for $a = b = 1$ and $d < e$ for a square lattice with $L = 50$ averaged over 500 realisations. The weights of the defects are indicated on the figure. The panels in the first row, (a) and (b), are for parameters such that $d > e^2$, with $e^2/d = 10^{-4}$ in (a) and $e^2/d = 10^{-2}$ in (b). The panels in the second row, (c) and (d), are for $d = e^2$.

As shown in Fig. 4 (a), for $d > e^2$ and large enough values of d , $d/e^2 \gtrsim 10^2$, the decay of n_e (green data points) and n_d (blue data points) freeze at a metastable density for around five decades in time. The density of e -vertices n_e is smaller than n_d in the plateau regime. Instead, still for $d > e^2$ but for smaller values of d , $d/e^2 \lesssim 10^2$, d -vertices rapidly disappear and the plateau is only seen on n_e , as shown in panel (b). Indeed, after a rapid decay, n_e gets frozen into a metastable value for a long time before it finally reaches its equilibrium value. Hence, one can conclude that the presence of d -defects in the system is *not* responsible for the emergence of the dynamical plateau in the total density of defects n_{def} .

The data in panels (c) and (d) in Fig. 4 were obtained for $d = e^2$. The density of n_e remains larger than n_d during the whole evolution in both cases. Similarly to what was observed for $e = d$ [11], the system gets blocked into a metastable plateau only for small enough values of $e \lesssim 10^{-4}$, and the existence of this arrested dynamical regime is not due to an excess of d -vertices. The evolution of n_e and n_d for $d < e^2$ shown in Fig. 4 supports this observation. Although n_d rapidly vanishes, n_e exhibits a dynamical arrest. The value of the plateau density can, in principle, depend on the weight of the vertices in a complicated manner. We did not study this last point in detail here.

In short, the system can be arrested in long-lived metastable states with many defects of type e .

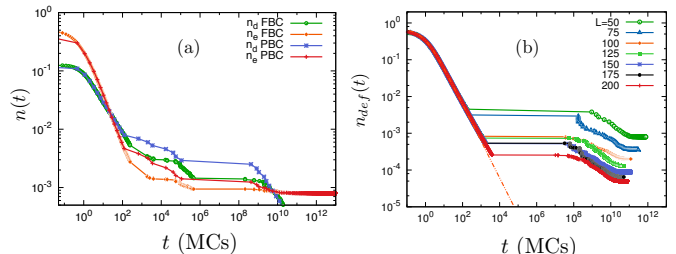


Figure 5. (Colour online.) Quench into the PM phase. (a) Time evolution of the density of defects, n_d and n_e , for different boundary conditions: periodic boundary conditions (PBC) and fixed boundary conditions (FBC). The data were obtained with an average over 500 realisations of the dynamics with $a = b = 1$ and $d = e = 10^{-7}$ for a system with linear size $L = 50$. (b) The time-dependence of the total density of defects, $n_{def} = n_d + n_e$, for different system sizes with PBC at $d = e^2 = 10^{-14}$, $a = b = 1$. The linear sizes are given in the key and vary by 25 from $L = 50$ to $L = 200$. The data were obtained after averaging over 300 runs. The initial decay of n_{def} is confronted to $\rho_0/(1 + \Omega t)$, with Ω a fitting parameter (red dotted line), see the text for a discussion.

3. Boundary conditions

In order to better understand the emergence of the frozen regime we repeated the numerical experiment with fixed boundary conditions (FBC): the state of each spin on the boundary is kept fixed from the one it had in the (random) initial configuration during the simulation. One has to be careful when choosing the boundary conditions and make sure that these do not induce a polarisation of the sample. Indeed, polarised boundary conditions such as the DWBC can have dynamical consequences such as the drift of defects (loosely speaking, magnetic monopoles). These effects have not been studied here.

In the initial high temperature state, defects of any kind populate the system. After the quench, one of the mechanisms for relaxation is the annihilation of oppositely charged defects. In order to do so, defects have to meet in the appropriate manner, meaning that the reversal of the spin shared by both of them restores the ice rule. In the reaction-diffusion language this corresponds to the process $(q) + (-q) \rightarrow (0) + (0)$. Two

defects of opposite charge ± 1 can also meet in the ‘wrong’ way and create, by a single spin-flip, a pair of doubly charged defects accordingly to: $(q) + (-q) \rightarrow (2q) + (-2q)$. Starting from a completely ordered FM configuration, one can create a pair of defects by flipping a string of spins. The latter can wind around the lattice by PBC. Then, in order to annihilate these pair of defects, one must flip back all the spins belonging to the string. One can imagine that this kind of extended structures could be responsible for the slowing down of the dynamics. If so, the evolution of the system with FBC, where winding strings are absent, should not present a dynamical plateau. As shown in Fig. 5 this is not the case: a metastable plateau in the evolution of the density of defects appears with FBC as well. This is due to the fact that, in the presence of more than a single pair of defects, there is always a way to annihilate all the defects without going through the boundaries of the lattice. In this sense, the dynamics are insensitive to the nature of the boundary conditions.

4. Finite size effects

As already pointed out in [11], the metastable density of defects for $d = e$ depends on the linear size of the system. One should then ask, for generic parameters, whether the observed metastable density is just a finite size effect or not. In order to give an answer to this question we simulated systems of different sizes under the same conditions that we chose to be $a = b = 1$ and $d = e^2 = 10^{-14}$. The results obtained are shown in Fig. 5 (b). The height of the plateau, n^p , and the time spent by the system in this regime decreases with the size of the system. However, as the plateau height is subject to strong fluctuations, we are not able to predict its precise dependence on the system size. The data do not show saturation at a finite value n^p nor length of the plateau and this gives a strong indication that this effect is due to the finiteness of the samples. This is confirmed by the data obtained after a quench into the c -AF phase for different system sizes (see Fig. 8): in this phase the data are less noisy and we found that the plateau density n^p depends on the size of the system as $\propto L^{-2}$ which vanishes in the thermodynamic limit. Having said this, we wish to stress that the system sizes of artificial spin-ice samples are of the same order as the ones used in our numerics and, therefore, blocking effects of the kind here shown are expected to exist in those samples as well, e.g. $L \approx 150$ in the samples studied in [2].

5. Initial decay

For $d = e$, see [11], the initial decay of n_{def} is well fitted by a power law decay

$$n_{def}(t) = \frac{\rho_0}{(1 + \Omega t)^\alpha} \quad (13)$$

with $\alpha = 0.78$. The evolution of n_e for $d = e^2$ shown in Fig. 5 (b) is rather well fitted by a diffusive decay $\rho_0/(1 + \Omega t)$. Interestingly, when $d \leq e^2$ the decay of the defects’

density agrees with the mean-field reaction-diffusion picture, $n_{def}(t) \simeq \rho_0/(1 + \Omega t)$, proposed in [27] for 3D dipolar spin-ice. The presence of d -defects modifies this behaviour and makes the decay slower [11], i.e. α decreases. This suggests that the exponent α depends on d/e^2 and crosses over from $\alpha = 1$ for $d/e^2 \ll 1$ ($d \leq e^2$) to $\alpha < 1$ beyond this limit.

B. Quench into the FM phase

We now turn to the ordering dynamics following a quench from a random initial condition into the FM phase dominated by a -vertices (i.e. $a \gtrsim b + 1 + d + 3e$ as discussed in detail in [12]). As shown in Fig. 6, a dynamic arrest occurs for small defects’ weights during the relaxation towards the a -FM phase as well. We anticipate that the same kind of behaviour also appears when the system is quenched into the c -AF phase (see Fig. 8).

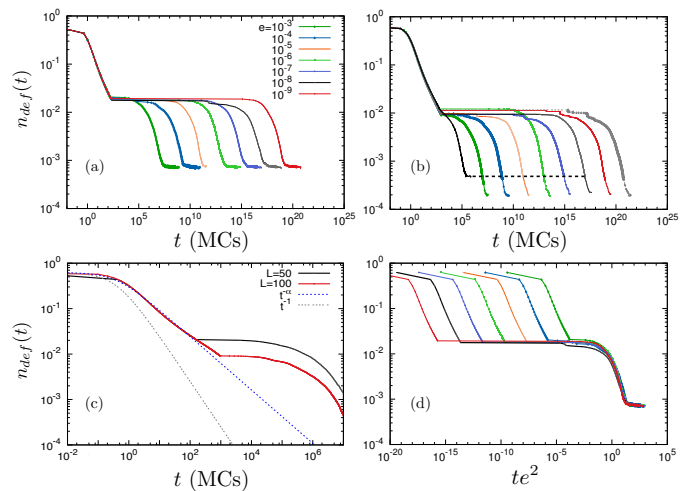


Figure 6. (Colour online.) Quench into the FM phase. Time dependent density of defects after a quench from $a = b = d = e = 1$ to $a = 5$, $b = 1$ and $d = e^2$ for the different values of e . (a) $L = 50$ and $e = 10^{-3}, 10^{-4}, \dots, 10^{-9}$ (as shown in the key). (b) $L = 100$ for $e = 10^{-2}$ (in black), $10^{-3}, \dots, 10^{-10}$. For $e = 10^{-2}$ the system saturates to its equilibrium value shown with a dotted black line. (c) Short-time behaviour for $e = 10^{-3}$, $L = 50$ and $L = 100$. The decay is confronted to $\rho_0/(1 + \Omega t)^\alpha$ (grey dashed line) and the fit $\rho_0/(1 + \Omega t)^\alpha$ with $\alpha = 0.59$ (blue dashed line). (d) Test of scaling with te^2 for $L = 50$.

In this section we analyse the relaxation towards the FM phase by studying the decay of the defects’ density for different values of the external parameters. In Fig. 6 we show the evolution of the density of defects after a quench to $a = 5$, $b = 1$, $d = e^2$ and different values of e for two different system’s sizes $L = 50$ (a) and $L = 100$ (b). The data shown have been averaged over 10^3 independent realisations of the dynamics. For small enough e ($e \lesssim 10^{-3}$) the system gets frozen into a metastable state with a finite density of defects. Similarly to what is observed after the quench into the PM phase [11], the time the system spends in this plateau is longer for smaller e . The ordering process following a quench into

the FM phase is characterised by a time scale $\tau \propto e^{-2}$ in the regime in which n_{def} leaves the plateau. As shown in Fig. 6 (d) for $L = 50$ all the curves collapse into a single curve when rescaling the time variable by τ . Therefore, the typical time associated with the creation of a pair of defects is the relevant time scale during this time regime.

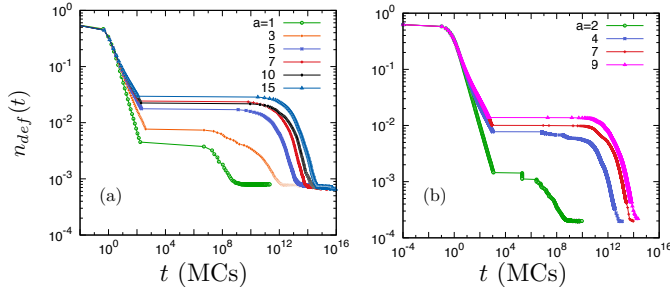


Figure 7. (Colour online.) Quench into the FM phase. Time-dependent density of defects after a quench from $a = b = d = e = 1$ to $b = 1, d = 10^{-18}, e = 10^{-6}$ and different values of a . (a) $L = 50$ for $a = 1, 3, 5, 7, 10, 15$ (as shown in the key). (b) $L = 100$ for $a = 2, 4, 7, 9$. The data have been averaged over 300 independent runs.

The evolution of the density of defects following a quench into different points of the a -FM phase is shown in Fig. 7 for $L = 50$ (a) and $L = 100$ (b) samples. During a short time regime ($t \lesssim 10$ MCs) the density of defects decays independently of a . For later times, the decay depends on the value of a . In particular, the expected power-law decay $n(t) \sim t^{-\alpha}$ becomes slower for larger values of a . Therefore, the exponent α depends on the weights of the vertices and decreases when increasing a . The metastable density of defects increases with a and depends on the system size.

The initial decay of n_{def} can be fitted by the power-law in eq. (13) with $\alpha \simeq 0.59$ over the whole time regime before the system reaches the plateau density [as shown in Fig. 6 (c)]. In the a -FM the decay becomes slower than the diffusive law, t^{-1} , found in the disordered phase. The algebraic decay does not depend on the size of the system as suggested by the data shown in Fig. 6.

A general statement can be made at this point: the value of the exponent α decreases - and hence the relaxation becomes slower - when going deeper into an ordered phase (of FM or AF kind).

C. Quench into the c -AF phase

We follow now the evolution of the system after a quench from a random initial condition into the AF phase dominated by c -vertices (i.e. $1 \gtrsim a + b + d + 3e$ [12]). Figure 8 displays the temporal dependence of the total density of defects, n_{def} , after such a quench for systems with different linear sizes given in the key. The inset shows the linear size dependence of the plateau height extracted from the data in the main part of the figure in a double logarithmic scale. The data points are accurately fitted by a L^{-2} dependence that suggests that

the plateau will disappear in the thermodynamic limit. The initial decay is algebraic with a non-trivial power $t^{-\alpha}$ with $\alpha = 0.74$ independently of the system size.

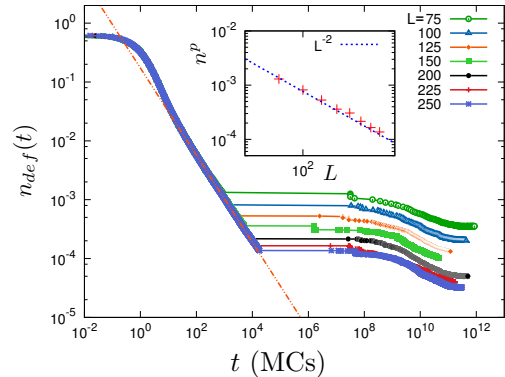


Figure 8. (Colour online.online.) Quench into the c -AF phase. Temporal decay of the density of defects in the system following a quench to the parameters $d = e^2 = 10^{-14}, a = b = 0.1$ and $c = 1$. The data plotted were obtained by using different lattice sizes $L = 50, \dots, 250$ and averaging over 300 independent realisations of the dynamics. The initial decay is confronted to the power-law decay $t^{-\alpha}$ with $\alpha = 0.74$.

D. Conclusion

In this section, we have shown that the system gets arrested into a long-lived frozen state for all kind of quenches as long as the weights e and d are small enough ($d \leq e \lesssim 10^{-4}$). After inspection of the persistence of the plateau for a large range of parameters and different boundary conditions, we concluded that the emergence of such dynamical arrest is not due to the presence of doubly charged defects and it is not an artifact of the periodic boundary conditions. The metastable density depends on the system size, in such a way that it might disappear in the thermodynamic limit. This assumption is supported by the L^{-2} dependence of the metastable density of defects after a quench into the c -AF phase (see Fig. 8). The scaling $n_{def}(t) \sim f(te^2)$ shown in Fig. 6 (d) gives a simple interpretation of the long time dynamics: the creation of a pair of defects is needed to ‘unblock’ the evolution and allows the system to reach its equilibrium state. Another result reported in this section concerns the initial decay of defects right after the quenches. We have shown that the density of defects follows a power-law decay characterized by an exponent α which depends on the vertex weights. In the PM phase, one recovers the mean field t^{-1} decay for $d \leq e^2$, as reported in 3D dipolar spin-ice [27]. For $d = e$ a smaller exponent $\alpha = 0.78$ was found [11], indicating that the relaxation is qualitatively slower. After a quench into the FM and AF phases the decay of defects becomes slower when choosing parameters deeper into the ordered regions of the phase diagram. For $a = 5, b = 1$ and $d = e^2 = 10^{-6}$ we found $\alpha = 0.59$ and we further showed that, at fixed value of b, d, e , this exponent decreases when increasing a .

IV. COARSENING DYNAMICS AND AGEING

In this Section we analyse the ordering process following a quench into the FM and AF phases from a totally random initial condition. We choose to work with defect weights satisfying $d = e^2$, differently from what we presented in [11], where $d = e$. The interest is to investigate the role played by each kind of defect in the ordering dynamics, for parameter that are closer to the experimental ones in ASI [4, 28].

A. Slow relaxation towards the PM phase

In Fig. 9 we show the decay of the two-time correlation function $C(t, t_w)$ as a function of the time difference $t - t_w$ for different values of t_w shown in the key, and working parameters such that $a = b = 1$ and $d = e^2$ (with different choices of the defect weights in the two panels, $d = e^2 = 10^{-4}$ in (a) and $d = e^2 = 10^{-12}$ in (b)). Recalling the results shown in Fig. 4 (c) and (d), metastability (a plateau in the number of defects) is not expected in (a) as the value of $d = e^2$ is sufficiently large, while it is expected after times, say, of the order of 10^4 MCs in (b) since $d = e^2$ it is pretty small ($e \leq 10^{-4}$).

One can distinguish different dynamical regimes from these curves. For short times, as long as neighbouring defects annihilate in a few MCs the correlations are time translational invariant and close to one. At later times time-translational invariance is lost and the system exhibits non-stationary relaxation. The longer the waiting-time t_w is, the slower the decay, as in an *ageing* situation.

In panel (a), when $d = e^2$ is relatively large, a stationary regime is attained for waiting-times of the order of $t_w \simeq 3 \times 10^5$ MCs as demonstrated by the fact that the two curves corresponding to the longest t_w , beyond this time-scale, fall on top of each other and do not depend on t_w . As shown in the figure, the equilibrium curve follows a stretched exponential decay: $C_{eq}(t, t_w) = F(t - t_w) = \exp[-(t - t_w)^\gamma / \tau_e]$ with $\gamma = 0.81$ and $\tau_e \approx 25 \times 10^3$ MCs. One could expect a similar picture away from the ‘spin ice’ ($a = b = 1$) curve $d = e^2$ in the disordered phase, with some dependence of the parameters t_{eq} , the relaxation time, γ , the stretching exponent and τ_e , the characteristic time. We have not studied these dependencies in detail.

The behaviour is different in panel (b), where the weight of defects is much smaller. The curves do not reach a stationary regime for the waiting times used. Moreover, a long plateau is seen in the curve for $t_w \approx 10^7$ MCs, reminiscent of the plateau in the decay of n_e shown in Fig. 4 (d). The system does not evolve during a period of time in between $\approx 10^7$ and 10^9 MCs. In this case an extremely long time-decay is necessary to reach a complete decorrelation. A steady state regime is not reached in the simulation, the correlations continue to evolve for all waiting times shown.

As argued in Sec. III, the finite size of the lattice has very strong effects in these systems. For larger system sizes the cross-over to metastability will be pushed to longer times, and to infinity in the thermodynamic limit. The ever-lasting non-stationary relaxation is due to the proximity to the spin-liquid

critical phase of the six vertex model when the defect weights are small enough. In any critical relaxation the system in question will grow equilibrium patches with a time-dependent critical length. This length will need an infinite time to reach the size of the system if this diverged.

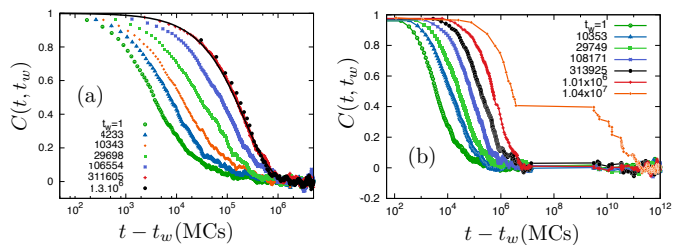


Figure 9. (Colour online.) Quench into the FM phase from a random initial configuration. Two-time self-correlation function $C(t, t_w)$ for a system with $L = 50$ and data averaged over 500 realizations. The system evolves with $a = b = 1$ and $d = e^2 = 10^{-4}$ in (a) while $d = e^2 = 10^{-12}$ in (b). Note that in both cases $d = e^2$. The equilibrium correlation function in (a) is confronted to $\exp[-(t - t_w)^\gamma / \tau_e]$ with $\gamma = 0.81$ and $\tau_e = 23014$ (solid black line), a law that describes the data very accurately.

B. Anisotropic FM domain growth

Starting from a random initial configuration, we quench the system by setting $a = 5$, $b = 1$ and $d = e^2 = 10^{-10}$ at $t = 0$. The equilibrium state corresponding to this set of parameters is deep into the FM phase. This choice strongly favours a -vertices. The system will then evolve towards its ordered FM state by growing domains made of type-1 and type-2 vertices.

A first hint into the dynamics of the system is given by the time evolution of the density of vertices, $n_\kappa(t)$, for each kind of vertex, $\kappa = a, b, c, d, e$. This is shown in Fig. 10. Differently from what we presented in [11] we distinguish here the density of each kind of defect as their weights are not the same. The data are accompanied by four configurations that illustrate the evolution of the system. One clearly observes the growth of anisotropic ordered FM domains. The directions \vec{u}_\parallel and \vec{u}_\perp defined in Fig. 1 are parallel and orthogonal to the longer domain walls, respectively.

From inspection of the data plotted in Fig. 10 we can identify four different dynamical regimes:

- (I) A short time regime ($t \lesssim 10^{-1}$ MCs) during which all densities vary very little (see, e.g., the data in [11] where we gave more data-points on this very short regime, for a different set of parameters).
- (II) An intermediate regime ($t \lesssim 10$ MCs) characterised by the annihilation of a large number of defects which are transformed into ice-rule vertices by a few single spin-flips. Then n_d and n_e decay (independently of the value of a , as shown in Fig. 7) while n_a , n_b and n_c increase. Quite surprisingly n_b and n_c increase in the same way in this regime. The typical configuration shows no apparent order although the tendency to align in a diagonal direction is already visible.
- (III) A slow relaxation regime in which the dominant dynamical

cal mechanism is the one of growing anisotropic FM domains made by type-1 (black) or type-2 (white) vertices. The third snapshot illustrates this situation: there is the same number of type-1 and type-2 vertices.

(IV) A much slower regime sets in once a FM domain percolates in the \vec{u}_{\parallel} direction. This regime is characterised by the emergence of very stable FM stripes ($t \gtrsim 10^3$ MCs). However, the sample is still very far from equilibrium as it needs to grow order in the \vec{u}_{\perp} direction as well in order to fully equilibrate. The percolation of a domain in this latter direction is achieved by a extremely slow mechanism that we describe below.

(V) The system equilibrates at much longer times ($t_{eq} \gtrsim 10^{11}$ MCs for this system size).

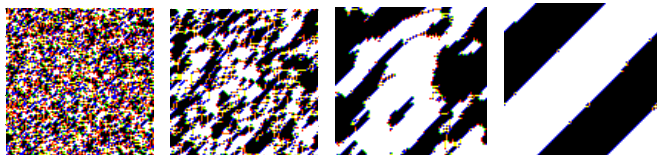
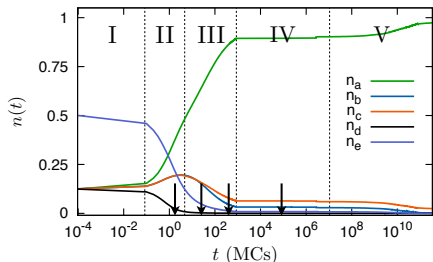


Figure 10. (Colour online.) FM ordering. Upper panel: time evolution of the density of vertices with weight a, b, c, d , and e for $a = 5$, $b = 1$, $d = e^2 = 10^{-10}$, in a system with linear size $L = 100$. The data are averaged over 300 samples. The snapshots are typical configurations at the instants indicated by the arrows. Black and white points are vertices 1 and 2 as defined by the colour code shown in Fig. 2.

The behaviour of the space-time correlation functions confirm this growth. As shown in Fig. 11 the correlations along the direction parallel to the stripes (b) grow faster than in the orthogonal direction (a). The function G^{\parallel} decreases monotonically and does not vanish at any distance for times larger than $\approx 10^3$ MCs (regime IV for which FM stripes percolate). Instead, the correlations along \vec{u}_{\perp} decrease rapidly at small distances and show a minimum at $L/(2\sqrt{2})$, then G^{\perp} increases. This is due to the tendency of the system to develop a modulated structure in time. Because of the periodic boundary conditions a stripe is constrained to wind around the lattice resulting in a modulated configuration (as illustrated by the right-most snapshot in Fig. 10). The growth is highly anisotropic since $a > b$. For $b > a$ correlations along u_{\perp} develop faster than along \vec{u}_{\parallel} , forming stripes perpendicular to the ones shown in Fig. 10. The relevant parameter characterising the anisotropy of the ordering process is the ratio a/b . As shown in the insets of Fig. 11, in the regime where anisotropic domains grow (regime III with times $t < 10^3$ MCs) the correlation function along both directions depends on space and

time through the ratio $r/t^{1/2}$:

$$G^{\perp, \parallel}(r, t) \simeq F^{\perp, \parallel}\left(\frac{r}{t^{1/2}}\right), \quad (14)$$

which confirms the growing length $L_{\perp, \parallel}(t) \sim t^{1/2}$ found for $d = e$ [11] with a less refined analysis. The master curves in the insets of Fig. 11 are confronted to $F^{\perp, \parallel}(x) = \exp[-(x/v_{\perp, \parallel})^{w_{\perp, \parallel}}]$ where $x = r/\sqrt{t}$. The best fits shown were obtained with $v_{\perp} = 0.89$, $w_{\perp} = 1.15$ (a) and $v_{\parallel} = 0.28$, $w_{\parallel} = 1.15$ (b). Notably, the stretching exponents w are the same (within numerical accuracy) but the scales $v_{\perp, \parallel}$ are different.

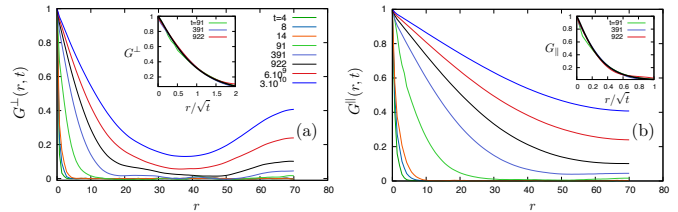


Figure 11. (Colour online.) Quench into the FM phase. Space-time correlation function along the orthogonal (a) and longitudinal (b) directions for $L = 100$, $a = 5$, $b = 1$, $d = e^2 = 10^{-10}$ and different times t given in the key. The data have been averaged over 300 runs. The insets show $G^{\perp, \parallel}$ as a function of the rescaled variable $r/t^{1/2}$ for different times in the coarsening regime III. The master curves in the insets are confronted to $F^{\perp, \parallel}(x) = \exp[-(x/v_{\perp, \parallel})^{w_{\perp, \parallel}}]$ where $x = r/\sqrt{t}$. The scaling functions $F^{\perp, \parallel}$ shown in thick black lines were obtained with $v_{\perp} = 0.89$, $w_{\perp} = 1.15$ (a) and $v_{\parallel} = 0.28$, $w_{\parallel} = 1.15$ (b).

The dynamical processes leading the dynamics during the different dynamical regimes can be understood from the analysis of the snapshots:

(i) As illustrated in Fig. 12, the topology of the model - i.e. the fact that a vertex of type-1 cannot have a neighbour of type-2 - leads to straight domain walls along the \vec{u}_{\parallel} direction made by c -vertices. Instead, the system would develop interfaces between FM states along the \vec{u}_{\perp} when quenched into the b -favoured FM phase. Plaquettes of ice-rule vertices, as shown in the central panel in Fig. 12, can frequently appear along the domain walls. The latter are obtained from the elementary excitations of the system. These ‘loop’ fluctuations are obtained by sequentially flipping the spins around a plaquette, an operation which preserves the ice-rule (see the first and second panel in Fig. 12).

(ii) Domains of the same type are connected by quasi-one-dimensional paths made of b - and c -vertices (loop fluctuation can eventually be attached to them as well) running through a region with the opposite order. The interplay between the tendency to order and the local constraint gives rise to these structures. They are similar to the ones found in the kinetically constrained spiral model [29]. In order to further increase the density of a -vertices and develop the FM order, the domain walls and strings of b - and c -vertices have to be eliminated. The latter disappear first via the following mechanism. Curved domains must have ‘corners’ made of b vertices or de-

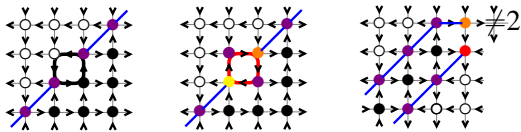


Figure 12. (Colour online.) Interfaces between FM domains. Local spins on the bonds and vertices are shown following the Colour rule established in Fig 2. Left panel: diagonal wall (blue solid line) separating two regions with opposite magnetisation both in the x - and y -directions. Central panel: a ‘loop’ fluctuation (red solid line) on the plaquette highlighted in the left panel. Right panel: a b corner vertex cannot be a neighbour of an a -vertex, illustrating the necessity of an outgoing string at the corner of an ordered domain.

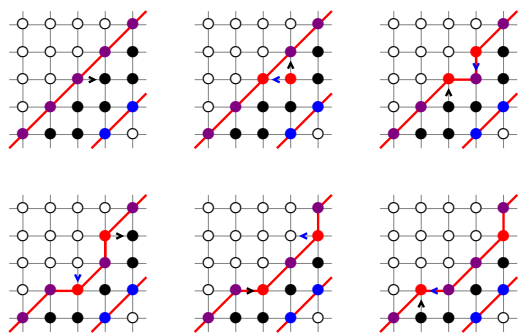


Figure 13. (Colour online.) Schematic representation of FM stripe motion. Vertices on each site are specified. Note that the interface is made of antiferromagnetic vertices. Diagonal (red) lines delimit domains of opposite magnetisation. Black arrows indicate the spins that flip to get the new configuration (represented in blue after the flip).

fects, but b vertices on the corners cannot be surrounded by more than two type 1 or 2 vertices (only defects can, giving rise to the before mentioned quasi one-dimensional structures, as illustrated in the third panel in Fig. 12). The string then progressively disappears eaten by the attached domains that grow from the corner or, alternatively, it is first cut by the creation of two defects and the two strands subsequently shrink. Once the string has been eliminated one is left with two defects sitting on the walls of the now detached domains, that move along the interface and eventually annihilate with their anti-partner.

(iii) Once the domains have grown enough to percolate in the \bar{u}_{\parallel} direction the mechanism sketched in Fig. 13 takes over. The formation of stable parallel stripes freezes the dynamics. The only way to evolve from a configuration with parallel FM stripes is to create a pair of defects by a single spin-flip. After the creation of a pair of defects on the domain wall, the diffusion of the latter along the interface shrink one among the two oppositely ordered stripes. This is illustrated by the sequence of steps in Fig. 13. The number of steps scales as the length of the stripe, hence the time associated to this process diverges with the size of the system.

C. Isotropic c -AF domain growth

We now turn to quenches into the AF phase. To start with we present results for parameters that favour isotropy, that is to say $a = b$, and defect weights such that $e > d$. This is the case realised in as-grown ASI samples [4, 28]. Next we show some snapshots for non-equal FM weights, $a \neq b$, though still in the AF phase to demonstrate that anisotropic AF growth is also possible.

1. c -AF sixteen-vertex model with $d = e^2$

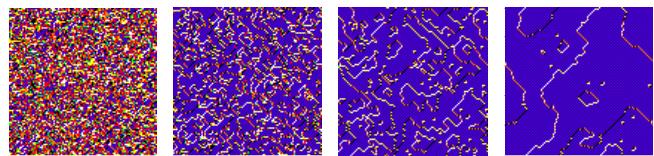
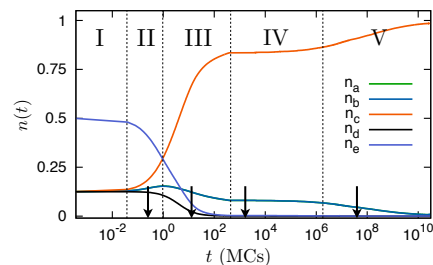


Figure 14. (Colour online.) c -AF ordering. Time evolution of the density of vertices in a system with $L = 100$ after a quench to $a = 0.1$, $b = 0.1$, $d = e^2 = 10^{-10}$ averaged over 500 runs. Snapshots taken at the instants indicated by arrows in the main panel are shown (using the colour code defined in Fig. 2).

In Fig. 14 we show the evolution of the vertex populations, n_{κ} , following a quench into the c -AF phase by setting $a = b = 10^{-1}$ and $d = e^2 = 10^{-10}$. This data are illustrated by configurations taken at different instants indicated by arrows in the main panel. This choice of parameters favours c -vertices and is invariant under $\pi/2$ -rotations. Therefore, the evolution proceeds by growing isotropic domains of opposite staggered magnetisation denoted by $m_{x,y}^{\pm} = \pm 1$ (the staggered orientation of the spins lying on horizontal and vertical edges respectively, see Fig. 1).

With a similar analysis to the one used for the FM quench, different dynamical regimes can be identified:

(I) A short transient where all the densities remain roughly constant.

(II) An intermediate regime ($t \lesssim 10$ MCs) with a rapid annihilation of defects into ice-rule vertices.

(III) A third regime during which $n_a = n_b$ decreases in order to grow isotropic c -ordered domains. The identity of a and b vertex weights implies that n_a and n_b are equal. This is explicitly shown by the data plotted in Fig. 15. The space-time self correlation functions along the \parallel and \perp directions are almost identical and the associated growing lengths are, within numerical accuracy, $t^{1/2}$. The scaling of the space-time cor-

relation function shown in the inset to panel (b) confirms this claim. Moreover, the scaling function is again a stretched exponential with an stretching exponent w that is very close to the one found in the FM quenches. The scale v depends on the working parameters. For these set of parameters and system size, regime III is relatively short, it lasts until $t \simeq 5 \cdot 10^2$ MCs.

(IV) Although we have not performed a full statistical analysis of this fact, it seems to us that the system freezes when an ordered structure winds around the finite size sample for periodic boundary conditions (or goes from one border to another for open boundary conditions). This regime is the one in which the plateau in the density of defects, discussed in the previous Section, emerges. In the plot in which we show the densities of each kind of vertices separately one sees that all densities are constant in this regime. The process whereby the system leaves this regime will be discussed below. The entrance into this regime will take longer times for larger sizes as already discussed in Sec. III.

(V) At longer times the system finally reaches equilibrium.

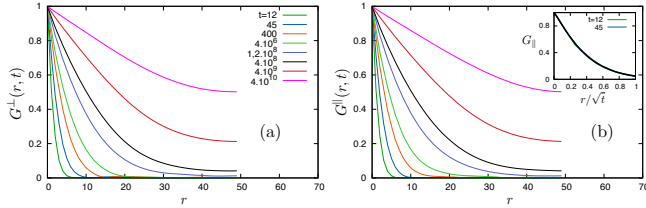


Figure 15. (Colour online.) Quench into the c -AF phase. Space-time correlations after a quench from a random initial condition into $a = 0.1 = b = 0.1$, $d = e^2 = 10^{-10}$ and $L = 50$ averaged over 500 runs. (a) Correlations along the \perp direction as a function of the distance r between sites for different times (shown in the key). (b) Correlations along the \parallel direction as a function of r for the same times as in (a). The inset shows the scaling of G^{\parallel} as a function of r/\sqrt{t} confronted to $g(x) = \exp[-(x/v)^w]$ with $x = r/\sqrt{t}$ (shown in thick black lines). The best fit shown in the inset was obtained with $v = 0.39$ and $w = 1.17$, that is very close to the value found for the stretching exponent in the FM phase.

A better understanding of the processes involved in the ordering dynamics is reached from the analysis of the snapshots.

(i) Domain walls are made of a - and b -vertices. Contrarily to the FM case, domains of any shape can be constructed without defects. As shown in the left and central panels in Fig. 16, horizontal and vertical walls are made by alternating a - and b -vertices. Diagonal walls are exclusively made by a - or b -vertices depending on their orientation. Therefore, domain walls without defects (energetically favoured) form loops of spins pointing along the same direction.

Dynamic domain walls in, say, Ising magnetic models with non-conserved order parameter (NCOP) dynamics are curved, and at finite times they display a variety of shapes, are relatively smooth at short length-scales and have fractal properties at long length-scales [30, 31]. Instead, in the sixteen-vertex model with $d = e^2 \ll 1$ c -AF domains have tendency to form straight walls made by FM vertices as shown

in the right most snapshot in Fig. 14. A statistical and geometric analysis of the morphology of domains and interfaces and their dependence on the parameters of the model remains an interesting project, especially if one wishes to confront the predictions of this model to images of artificial spin ice samples.

(ii) In the Solid-on-Solid (SOS) representation of the six-vertex model [32], each domain can be interpreted as a contour line delimiting regions with different height. The ordering then proceeds by growing or shrinking regions of constant height. Note that the Kosterlitz-Thouless phase transition of the F-model ($a = b$) can be mapped onto the roughening transition [32]. The ordering dynamics in this phase thus correspond to flatten the initial rough surface by growing regions made by c -vertices.

(iii) Once isotropic domains are created, one has to eliminate small domains in order to further increase the density of c -vertices of the losing kind and develop the conquering c -AF order. Figure 17 illustrates the mechanism taking place. After the creation of a pair of defects in a typical time $\sim 1/e^2$, their motion along the wall shrinks the domain. This is done without any energy cost and the sequence of steps needed to make a domain disappear should scale with its size. The same kind of mechanism takes place for horizontal domain walls.

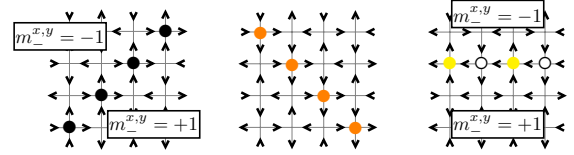


Figure 16. (Colour online.) Domain walls between c -AF domains of opposite staggered order. The configuration of arrows is shown. We use the colour rule defined in Fig. 2. Left panel: diagonal walls in the \parallel direction are made of a -vertices. Central panel: diagonal walls in the \perp direction are made of b -vertices. Right panel: horizontal (and vertical, by symmetry) walls are made of an alternating chain of a - and b -vertices.

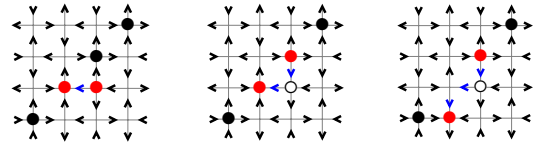


Figure 17. (Colour online.) Schematic representation of the annihilation of c -AF domains. Vertices on the walls are represented by the colour rule defined in Fig. 2. Blue arrows indicate the spins that have been flipped to get the new configuration. As defects diffuse along the domain wall the ordered region on the right-bottom side of the figure shrinks.

2. Artificial Spin Ice

As shown in [19], one can choose the vertex weights $c > a = b > e > d$ in order to model as-grown ASI samples [4, 28]. In these experiments, ferromagnetic islands are gradually grown by deposition. During the early stages of the preparation the system feels thermal fluctuations and thus tries to accommodate to its c -AF ground state. Once the islands reach a critical size the system blocks into a frozen configuration. The question as to whether such frozen configurations sample the equilibrium distribution has been recently addressed experimentally [4, 28] and theoretically [19]. Using this latter choice of parameters inspired by ASI samples: $a = \exp(-\beta\epsilon_a)$, $b = \exp(-\beta\epsilon_b)$, $c = \exp(-\beta\epsilon_c)$, $d = \exp(-\beta\epsilon_d)$ and $e = \exp(-\beta\epsilon_e)$, with $\epsilon_a = \epsilon_b = 2/l$, $\epsilon_c = 2(1 - 2\sqrt{2})/l$, $\epsilon_d = 2(2\sqrt{2} + 1)/l$ and $\epsilon_e = 0$ (l being the lattice constant); the AF domain walls become smoother than the ones obtained for $d = e^2 = 10^{-10}$. It is due to the presence of more defects lying on the interfaces (see Fig. 6 in [19]). This kind of domain wall pattern has also been observed in as-grown artificial spin-ice samples [4]. This is why we believe that some of these samples, the ones that are close to the phase transition, are out of equilibrium although the density of defects is notably well described by the model in equilibrium [12] and in simulation studies of a spin-ice model system [16].

Therefore, the shape of the interfaces separating opposite AF regions is extremely sensitive to the choice of parameters. Setting a slightly above (below) b would produce a preference to grow domains in the \vec{u}_{\parallel} (\vec{u}_{\perp}) direction. This is illustrated by the two snapshots shown in Fig. 18. As shown in [12], the equilibrium fluctuations of the model reflect this feature as well. The evolution of the system after a quench into the c -AF phase would eventually get frozen into an extremely slow relaxation regime, due to the presence of percolating domains in the \vec{u}_{\parallel} (\vec{u}_{\perp}) direction. The anisotropic dynamical scaling is difficult to study with our numerical methods in this case, and it is not clear whether the same scaling ($L_{\parallel} \sim t^{1/2}$) holds along both directions. Experimentally, the anisotropy ratio a/b can be tuned by placing islands of different length along the horizontal and vertical edges. This work should incite experimentalists to study this rich far from equilibrium behaviour in ASI.

V. CONCLUSION

In this paper we presented a thorough study of the relaxational stochastic dynamics of the sixteen vertex model with low defect weights after quenches from infinite temperature to the three equilibrium phases: disordered, ferromagnetic and antiferromagnetic ones.

In [11, 12, 19] we proposed that this celebrated model captures many important aspects of two dimensional artificial spin ice systems. The interest in these materials lies on the fact that they are a possible new technology for storage data devices. Our approach to these systems is, clearly, theoretical as their fabrication and preparation pose a number of rather

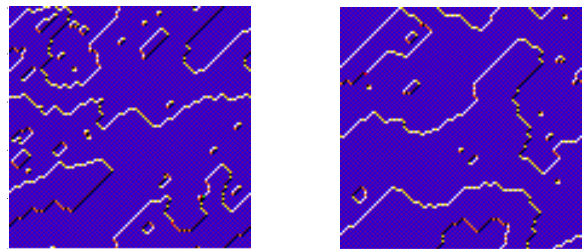


Figure 18. (Colour online.) Typical configurations of an $L = 100$ lattice with $a = 0.1$, $b = 0.01$, $d = e^2 = 10^{-10}$ (left) and $a = 0.1$, $b = 0.001$, $d = e^2 = 10^{-10}$ (right). The two snapshots have been taken at different times during the ordering regime IV in the c -AF phase.

fundamental questions that we can try to give an answer to by better understanding the behaviour of the model.

In the present publication we showed that, for sufficiently low defect weight and finite though large system size, the single spin-flip stochastic dynamics of the model that mimics thermal agitation in artificial spin ice, after quenches from infinite temperature, present several, very distinct, collective dynamic regimes. In short, these regimes are the rapid annihilation of defects at very short time scales, coarsening of nearly critical or phase ordering kind in the paramagnetic or ordered phases, respectively, metastability over a very long period of time, and the final approach to equilibrium. The coarsening process in the paramagnetic phase is controlled by the proximity of the critical phase in the absence of defects, the so-called spin-liquid phase of the six vertex model. The phase ordering kinetics in the ferromagnetic phases is characterised by anisotropic growth of the ferromagnetic equilibrium states related by spin-reversal. The ordering process in the anti-ferromagnetic phase is isotropic for parameters belonging to the so-called F-model ($a = b$) but it is not isotropic for other choices of weights.

In quenches to the FM phase we found that the end of the first coarsening regime is attained when two diagonal stripes of opposite ferromagnetic order percolate across the sample. Note that these states are equivalent from a thermodynamic point of view and no interaction in the model's Hamiltonian distinguishes between them. It is the dynamics that develops this transient, although very long-lived, anisotropy. The crossover from coarsening to metastability clearly depends on the size of the sample and the growth law $t^{1/2}$ suggests a crossover-time $t_{co} \simeq L^2$ when an ordered band goes from one system border to another. The fact that the dynamics get blocked with *two* stripes is based on the visual analysis of the snapshots and the fact that the perpendicular space-time correlation reaches a minimum at a distance of the order of $L/(2\sqrt{2})$. A more refined analysis along the lines in [33, 34] is necessary to clarify the role played by the initial condition in the number of stripes in the blocked state. As the time needed to let the stripes percolate across the sample diverges with the system size, it is clear that metastability and the further approach to equilibrium (regimes IV and V) are pushed to infinity in the thermodynamic limit.

In quenches to the c -AF phase the entrance in the metastable regime is also achieved when the two domains with the opposite staggered magnetisation percolate and, therefore, the last two regimes are moved to divergent time-scales in the thermodynamic limit in this phase as well. AF ordering is characterised by a $t^{1/2}$ growing length.

In quenches to the PM phase, the proximity to the critical spin-liquid of the six vertex model leads to a relaxation with a very long relaxation time that diverges in the limit of zero defect weight. Equilibrium patches are hard to visualise in a model with many local variables as the single vertices we have in this model but, most probably, the cross-over to metastability is also controlled by percolation of one (or more) of these regions in this phase. A critical growing length that should saturate to a finite value should exist in this regime as well.

We found stretch exponential scaling functions for the space-time correlation functions in the two anisotropic directions during FM coarsening and in the isotropic AF coarsening. The fits are consistent with the same (within numerical accuracy) stretching exponent w but different scale v , i.e. for a scaling function $F(x) \simeq \exp[-(x/v)^w]$.

Long-lived metastable states exist in the three phases after a cross-over time that should diverge with the system size. Still, as artificial spin-ice samples are of finite size, we studied these states in detail here. The configurations found in these time scales, that we called regime IV in the Sections concerning the ordered phases, are characterised by densities of each kind of vertex that are still far from their equilibrium values for the parameters that we investigated in this paper (note, however, that agreement between dynamic and static densities of vertices can be achieved for other parameters, as some of the ones used in [12] with the aim of confronting to experimental data). In particular, we found here a finite number of defects in the dynamic configurations. Our finite size scaling analysis suggests that their density vanish in the infinite size limit though it is hard to reach a definite conclusion in this respect.

Regime IV is succeeded by a totally different epoch during which complete ordering is eventually reached. Several mechanisms for the motion of domain walls in the FM and AF phases that constitute the relevant relaxation processes in this time regime have been identified and discussed in the text.

Let us conclude by confronting our approach to other dynamic studies of the same physical problem, reported in the literature in the last two or three years. Metastability in the defect density of frustrated magnets was discussed in [27] by using a reaction-diffusion model in which the defects are represented by charges and interactions of Coulomb type are considered. In this modelling the ‘background configuration’ is not taken into account. In our model, instead, the structure in which the defects are placed and displace is very important and determines the crossover time to metastability, the frozen nature of the system, the escape time from this frozen state and the subsequent final relaxation to equilibrium. In [16], a mean-field model of spin-ice, with only short range interactions, is proposed in order to study the domain wall dynamics of ASI in the presence of disorder and magnetic fields, two ‘external’ perturbations that we have not taken into account in our work. A very different approach has been taken in [10] to address spin-ice dynamics in $2D$. In this work the authors introduce a model of continuous magnetic moments with dipolar interactions and study its stochastic dynamics. The strong anisotropy imposed along the edges of the underlying square lattice makes the connection with ASI samples possible. From a more general perspective on $2D$ frustrated magnetism, numerical studies of the constrained dynamics of a simple classical lattice model have shown the existence of a dynamical arrest analogous to the one discussed in the text [24]. In this work the defects breaking a local constraint (analogous to the ice-rules) are strictly forbidden contrarily to what we do in our paper. Our work presents a new approach that allows to deal with thermal fluctuations breaking a hard constraint, and its consequences in the out-of-equilibrium relaxation of geometrically frustrated magnets.

-
- [1] L. BALENTS, *Nature* **464**, 199 (2010).
- [2] R. F. WANG, C. NISOLI, R. S. FREITAS, J. LI, W. MCCONVILLE, B. J. COOLEY, M. S. LUND, N. SAMARTH, C. LEIGHTON, V. H. CRESPI, and P. SCHIFFER, *Nature* **439**, 303 (2006).
- [3] C. NISOLI, R. WANG, J. LI, W. MCCONVILLE, P. LAMMERT, P. SCHIFFER, and V. CRESPI, *Phys. Rev. Lett.* **98**, 217203 (2007).
- [4] J. P. MORGAN, A. STEIN, S. LANGRIDGE, and C. H. MARROWS, *Nature Phys.* **7**, 75 (2010).
- [5] R. P. COWBURN and M. E. WELLAND, *Science* **287**, 1466 (2000).
- [6] S. D. BADER, *Rev. Mod. Phys.* **78**, 1 (2006).
- [7] M. J. HARRIS, S. T. BRAMWELL, D. F. MCMORROW, T. ZEISKE, and K. W. GODFREY, *Phys. Rev. Lett.* **79**, 2554 (1997).
- [8] S. T. BRAMWELL, M. J. P. GINGRAS, and P. C. W. HOLDSWORTH, in *Frustrated spin systems*, edited by H. T. DIEP, World Scientific, 2004.
- [9] G. MÖLLER and R. MOESSNER, *Phys. Rev. Lett.* **96**, 237202 (2006).
- [10] G. M. WYSIN, W. A. MOURA-MELO, L. A. S. MÓL, and A. R. PEREIRA, *arXiv:1208.6557* (2012).
- [11] D. LEVIS and L. F. CUGLIANDOLO, *EPL* **97**, 30002 (2012).
- [12] L. FOINI, D. LEVIS, M. TARZIA, and L. F. CUGLIANDOLO, *J. Stat. Mech.*, P02026 (2013).
- [13] R. J. BAXTER, *Exactly solved models in statistical mechanics*, Dover, 1982.
- [14] E. H. LIEB and F. Y. WU, in *Phase transitions and critical phenomena Vol. 1*, edited by C. DOMB and J. L. LEBOWITZ, chapter 8, Academic Press, 1972.
- [15] R. J. BAXTER, *Phys. Rev. Lett.* **26**, 832 (1971).
- [16] Z. BUDRIKIS, K. L. LIVESSEY, J. P. MORGAN, J. AKERMAN, A. STEIN, S. LANGRIDGE, C. H. MARROWS, and R. L. STAMPS, *New J. Phys.* **14**, 035014 (2012).
- [17] J. D. BERNAL and R. H. FOWLER, *J. Chem. Phys.* **1**, 515 (1933).
- [18] L. PAULING, *J. of Chem. Phys.* **57**, 2680 (1935).

- [19] D. LEVIS, L. F. CUGLIANDOLO, L. FOINI, and M. TARZIA, *arXiv:1302.3725* (2013).
- [20] I. A. RYZHKIN, *J. Exp. Theor. Phys.* **101**, 481 (2005).
- [21] C. CASTELNOVO, R. MOESSNER, and S. SONDHI, *Nature* **451**, 42 (2008).
- [22] A. B. BORTZ, M. H. KALOS, and J. L. LEBOWITZ, *J. Comp. Phys.* **17**, 10 (1975).
- [23] B. CHAKRABORTY, D. DAS, and J. KONDEV, *Eur. Phys. J. E* **9**, 227 (2002).
- [24] O. CEPAS and B. CANALS, *Phys. Rev. B* **86**, 024434 (2012).
- [25] V. KOREPIN and P. ZINN-JUSTIN, *J. Phys. A* **33**, 7053 (2000).
- [26] P. ZINN-JUSTIN, *Phys. Rev. E* **62**, 3411 (2000).
- [27] C. CASTELNOVO, R. MOESSNER, and S. L. SONDHI, *Phys. Rev. Lett.* **104**, 107201 (2010).
- [28] J. P. MORGAN, J. AKERMAN, A. STEIN, C. PHATAK, R. M. L. EVANS, S. LANGRIDGE, and C. H. MARROWS, *Phys. Rev. B* **87**, 024405 (2013).
- [29] F. CORBERI and L. F. CUGLIANDOLO, *J. Stat. Mech.*, P09015 (2009).
- [30] J. J. ARENZON, A. J. BRAY, L. F. CUGLIANDOLO, and A. SICILIA, *Phys. Rev. Lett.* **98**, 145701 (2007).
- [31] A. SICILIA, J. J. ARENZON, A. J. BRAY, and L. F. CUGLIANDOLO, *Phys. Rev. E* **76**, 061116 (2007).
- [32] H. VAN BEIJEREN, *Phys. Rev. Lett* **38**, 993 (1977).
- [33] K. BARROS, P. L. KRAPIVSKY, and S. REDNER, *Phys. Rev. E* **80**, 040101 (2009).
- [34] T. BLANCHARD and M. PICCO, *arXiv:* (2013).